Modified compact tension specimen for experiments on cement based materials: comparison of calibration curves from 2D and 3D numerical solutions

S. Seitl, V. Viszlay
Brno University of Technology, Faculty of Civil Engineering, Veveří 331/95, Brno 602 00, Czech Republic
Seitl.s@fce.vutbr.cz, http://orcid.org/0000-0002-4953-4324, viszlay.v@fce.vutbr.cz

ABSTRACT. The evaluation of fracture mechanics parameters of materials has become very important part of considering the condition of older constructions as well as properties of newly developed materials. This contribution focuses on a numerical simulation and a calculation of fracture mechanical properties of modified compact tension test configuration. It is possible to prepare the specimens used for this test very easily from a drilled core or from specimens used for cylindrical compression test. The focus of contribution is to compare selected outputs from numerical solution of 2D (plane strain conditions) with 3D models. Particularly, the determination of the influence of 2D and 3D model on the calibration curves for selected fracture mechanics parameters is of interest. Finite element software ANSYS was used for the numerical analysis.

KEYWORDS. Stress Intensity Factor; COD; CMOD; Biaxiality Factor; Modified Compact Tension Test; Fracture Mechanics of Concrete.

Citation: Seitl, S., Viszlay, V., Modified compact tension specimen for experiments on cement based materials: comparison of calibration curves from 2D and 3D numerical solutions, Frattura ed Integrità Strutturale, 39 (2017) 118-128.

Received: 17.07.2016
Accepted: 22.09.2016
Published: 01.01.2017

INTRODUCTION

Compact tension (CT) tests have been widely and successfully applied for measuring the fracture properties of several materials, such as metals (ASTM Standard E-399 [3]), or even composite materials with limited orthotropy [1]. Note that for test of fracture properties is not prepared norm only recommendation RILEM for three point bending test [17], RILEM for bending test for concrete with fibers [16, 18] and as a standard test the wedge splitting test is used (cube or cylindrical [12, 14, 19, 20]). The compact tension fracture toughness test (CT test [11, 22]) is essentially performed by applying equal and opposite forces through two holes previously made in the specimen, to propagate an initial crack. However, its applicability in concrete is characterized by some disadvantages, such as drilling the holes necessary to apply

the pulling forces and the hazard of a local fracture originated at these holes. The modified compact tension test (MCT [4, 5, 9, 10, 21, 23) is a quite new test configuration on notched specimens to obtain fracture mechanics parameters of materials in laboratory conditions, note that test is derived from classic CT test. A detailed research program/campaign has to be done before the configuration starts to be used as a standard.
The several authors used cohesive crack model and prepared MCT model in software ATENA [10] or in software ABAQUS [5]. Pilot experimental measurement and comparison of selected configurations with three point bending specimen is introduced in contributions [4, 9].
The main advantage of MCT test is a round shape of the specimen that makes it appropriate for testing cement based composites. Due to its shape, it is easy to prepare specimen both ways: by cutting them of the drilled core in case of constructions which are already being used [6-8, 15,] as well as in forms from the fresh concrete mixture [24]. The geometry of the specimen is shown in Fig. 1.

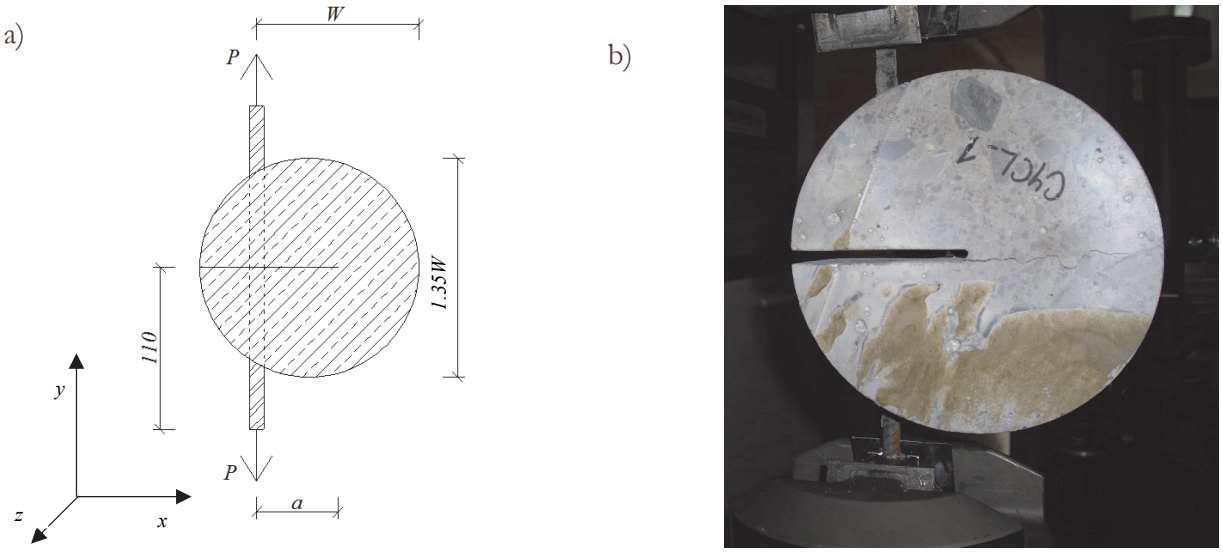

Figure 1: Modified compact tension test: a) schema of the test and b) a photo from the test.

The aim of the paper is to provide calibration curves according to four different fracture mechanics parameters and to compare selected case with the values obtained from 3D model with the results from 2D model, which have already been published in [21]. The first considered parameter is stress intensity factor K_I [MPa·m$^{1/2}$], see e.g. [1, 3, 11]. The value of stress intensity factor for each normalized crack length a/W is obtained by linear extrapolation from values in particular nodes behind the crack tip up to 3 mm distance. Values in a number of first nodes had to be neglected due to big mistake caused by stress singularity near to the crack tip. Values of T-stress [MPa] defined e.g. were obtained by different method. Both parameters were normalized as dimensionless biaxiality factors B_1 [-] and B_2 [-] by (1) using the Eqs. (2) and (3), see [11, 13]:

$$K_0 = \frac{P}{t\sqrt{W}}, \tag{1}$$

$$B_1 = \frac{K_I}{K_0}, \tag{2}$$

$$B_2 = \frac{T\sqrt{\pi a}}{K_I}, \tag{3}$$

where P is loading force in [N], t is thickness of the specimen in [mm], W stands for the position of loading force in [mm] and a is the crack length in [mm].

The next two considered parameters were opening displacements. The first, crack opening displacement COD [mm] is an opening displacement under the load force (at loadline), 5 mm from the crack path. The second one, crack mouth opening displacement CMOD [mm] is measured at crack edge. In both cases, the outputs were dimensionless compliance functions $f_{COD}(a/W)$ [-] and $f_{CMOD}(a/W)$ [-] obtained from measured values of displacement by using normalization Eq. (4) in the Eq. (5).

$$f_{norm} = \frac{K_I \sqrt{a/W}(1+\upsilon)}{2E\sqrt{2\pi}}, \tag{4}$$

$$f(a/W) = \frac{u_y}{f_{norm}}, \tag{5}$$

where u_y is selected point displacement in [mm], υ is Poisson's ratio [-] and E is Young's modulus [MPa]. The positions of selected points are related to the experimental set-up position: CMOD-clip gage at the end of specimen and COD – by displacement of machine load set up or both (CMOD, COD) points by system ARAMIS or other digidal image correlation system. The considered values of material characteristics are sumarized in Tab. 1.

Elastic properties	E [MPa]	ν [-]
Steel	210 000	0.3
Concrete - 5	5 000	0.2
Concrete - 20	20 000	0.2
Concrete - 25, see [21]	25 000	0.2
Concrete - 60	60 000	0.2
Concrete - 100	100 000	0.2

Table 1: Characteristics of used materials as the input parameters for numerical calculation.

NUMERICAL SOLUTION

In this paper, the 2D and 3D models for numerical solution will be compared in a range of two-parameter fracture mechanics (see [11, 20]). The finite element software ANSYS was used for numerical analysis [2]. Element type PLANE183 was used for 2D simulation which is able to degenerate from 8-node to 6-node and therefore is able to fit better stress singularity due to translocate to middle node to ¼ distance from crack tip. For 2D model, the plane-strain conditions were applied due to experiment specimen thickness 50 mm. The 2D solution is described and discussed in [21]. For 3D model, the element SOLID186 was used. This type of element is suitable for irregular meshes, tetrahedral and pyramid options could be used. The specimen thickness for 3D model was 50 mm (full specimen).

A diameter of specimen used for simulations was selected as D=150 mm as an appropriate size of a drill which is commonly used to obtain this type of specimen from a construction element. A considered length of the steel bars was 110 mm on each side of the specimen and used load force was P=1500 N. The load force was applied as a pressure on the area at the end of the bar so the stress was applied uniformly. The end part of the steel bar (last 30 mm) was considered to be gripped into hydraulic testing machine. Therefore for this part, a displacement in x and z directions was set to zero. The diameter of the steel bars was 8 mm. An interface among the steel bar and a concrete matrix was modeled without any transitional layer (perfect adhesion). The perpendicular distance between steel bars and the middle of the specimen was 45 mm. A relative crack length α (stands for a/W ratio) varied from 0.1 to 0.9 in steps of 0.1.

The density of the mesh was refinded in the vicinity of the crack tip, where average element size was 0.2 mm. Then the element size fluently increases to the value of 5 mm on the outer sides of the specimen. The advantage of symmetric specimen was exploited and so only 1/4 of 3D model was built. The symmetric boundary conditions were applied along the vertical cross-section.The meshed model for α=0.4 is shown in Fig. 2.

NUMERICAL RESULTS AND DISCUSSION

The finite element simulations were performed for various values of material properties listed in Tab. 1 (effect of change elasticity modulus ratio – constant value of Young's modulus for steel and the value of Young modulus for concrete is changed), and effect of 2D and 3D model solutions for various crack lengths, subjected to uniform load. The results of stress intensity factors K and T-stress are normalized by Eq. (2) and (3). In Figs. 3 and 8, the examples of deformed finite element models of 2D and 3D solutions are shown. The calibration curves are introduced in Eqs. (6-24) for each selected case.

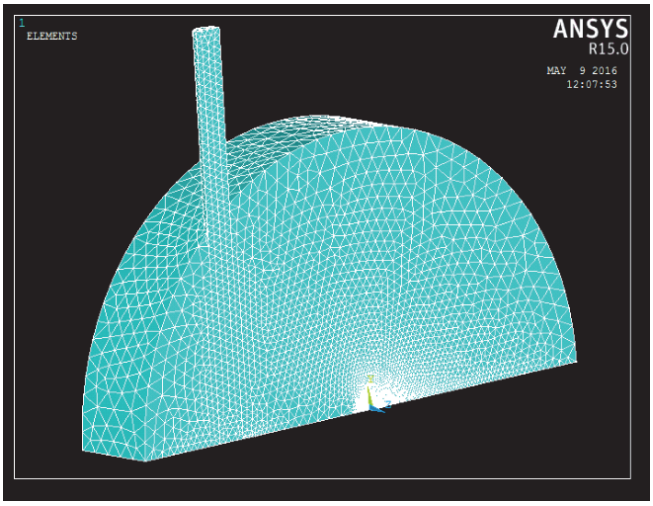

Figure 2: Example of finite element 3D model used for numerical study α=0.4.

Effect of elasticity modulus ratio

The numerically obtain results from 2D model solution covering the effect of elastic modulus ratio are shown in Figs. 4-7 (stress intensity factor, T-stress, COD and CMOD). The results of stress intensity factors and T-stress are normalized by Eqs. (2) and (3).

The functions of the calibration curve for MCT specimens with steel bars with diameter 150 mm have to be calculated for each value of Young's modulus, especially, for long cracks from 0.6 to 1, see example for selected values.

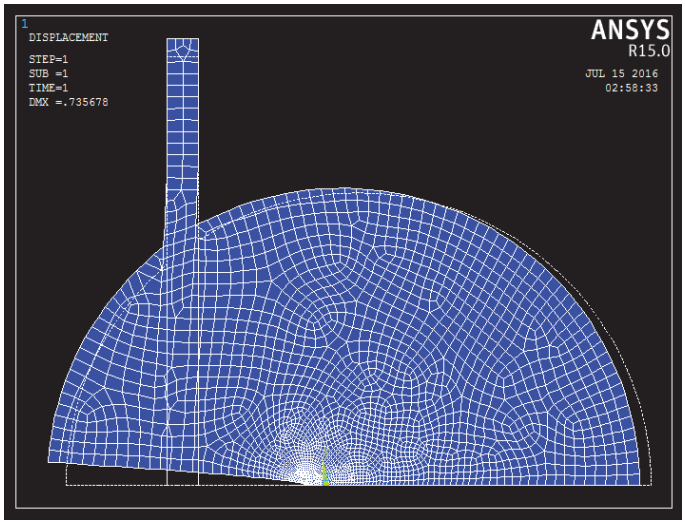

Figure 3: Example of 2D finite element model after deformation.

The B_1 curves are practically the same values for all five various materials. It only changes for values of relative crack length longer than α =0.5 (see Fig. 4). The functions of calibration curves for selected Young's modulus of concrete E= 5, 20 and 100 GPa can be introduced as follows:

$$B_1\ (E=5) = 5.5881 - 34.181\alpha + 239.39\alpha^2 - 594.79\alpha^3 + 688.58\alpha^4 - 251.61\alpha^5 \quad (6)$$

$$B_1\ (E=20) = -2.3617 + 117.22\alpha - 736.11\alpha^2 + 2191.5\alpha^3 - 2926.8\alpha^4 + 1503.9\alpha^5 \quad (7)$$

$$B_1\ (E=100) = -16.91 + 389.22\alpha - 2465.6\alpha^2 + 7030.8\alpha^3 - 9049.3\alpha^4 + 4371.4\alpha^5 \quad (8)$$

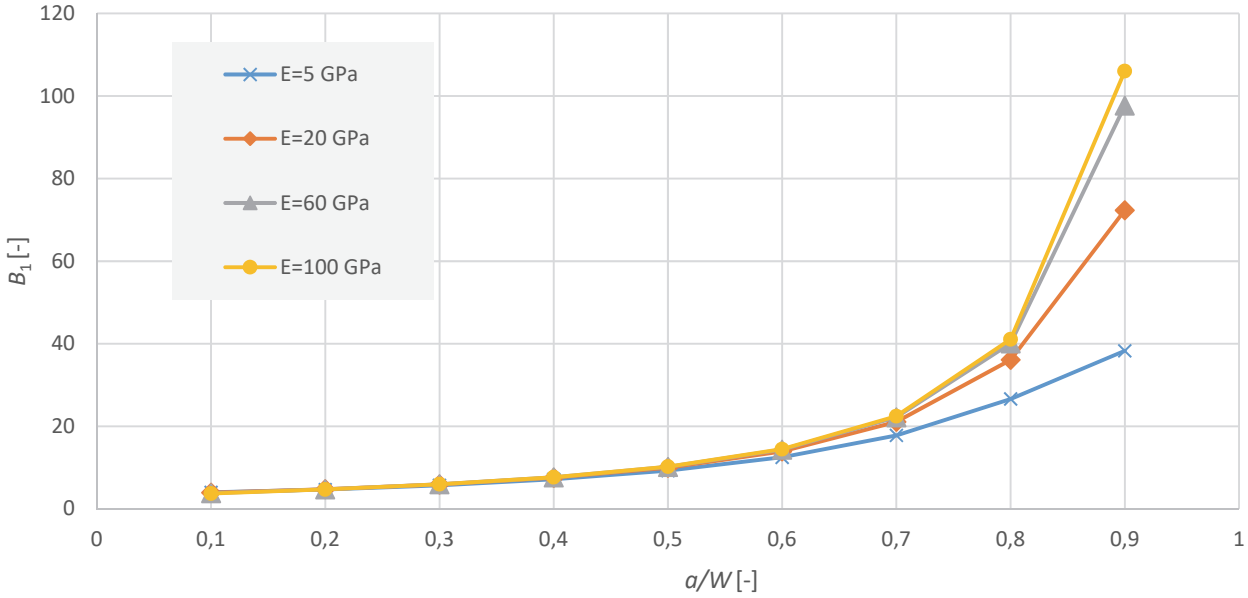

Figure 4: Values of dimensionless B_1 factor (stress intensity factor) versus a/W, the effect of elasticity modulus ratio (steel E=210 GPa).

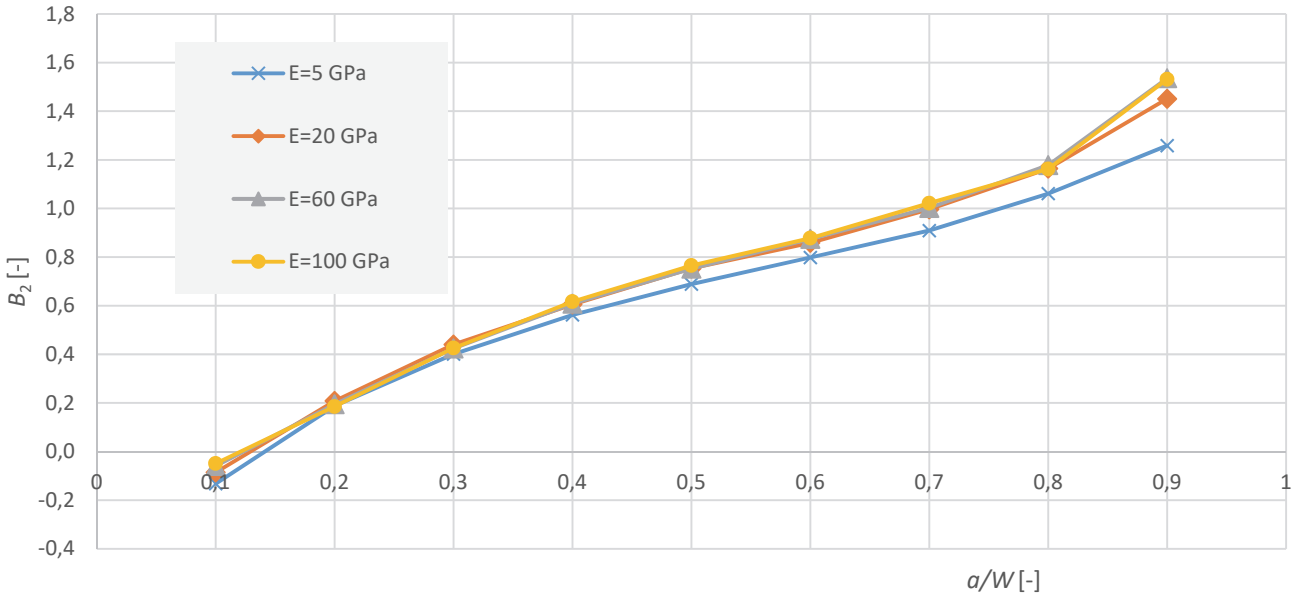

Figure 5: Values of dimensionless B_2 factor (T-stress) versus a/W, the effect of elasticity modulus ratio (steel E=210 GPa).

Fig. 5 shows that the B_2 parameter changes practically negligibly, only for very low values of Young's modulus E=5 GPa, there is relatively small deviation from another curves.

$$B_2\,(E=5) = -0.5625 + 5.0149\alpha - 7.4585\alpha^2 + 5.1659\alpha^3 - 0.636\alpha^4 \quad (9)$$

$$B_2\,(E=20) = -0.4339 + 3.7445\alpha - 2.3166\alpha^2 - 2.6828\alpha^3 + 3.5752\alpha^4 \quad (10)$$

$$B_2\,(E=100) = -0.2136 + 1.0257\alpha + 7.8949\alpha^2 - 17.492\alpha^3 + 10.933\alpha^4 \quad (11)$$

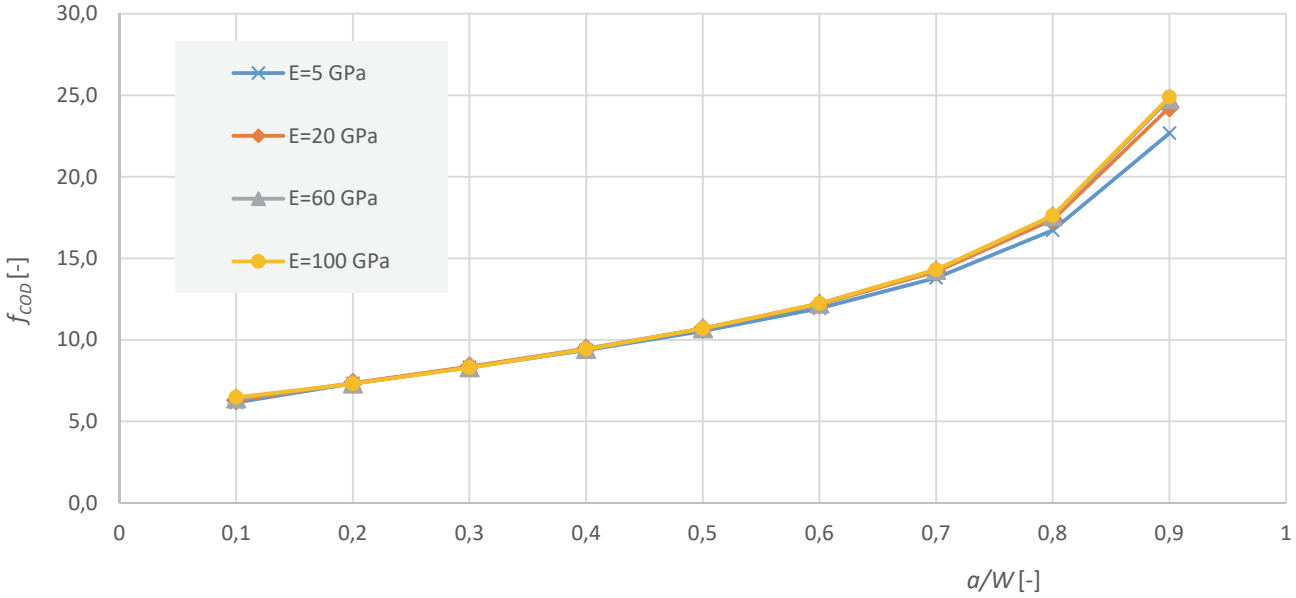

Figure 6: Values of COD (opening at load line) versus a/W, the effect of elasticity modulus ratio (steel E=210 GPa).

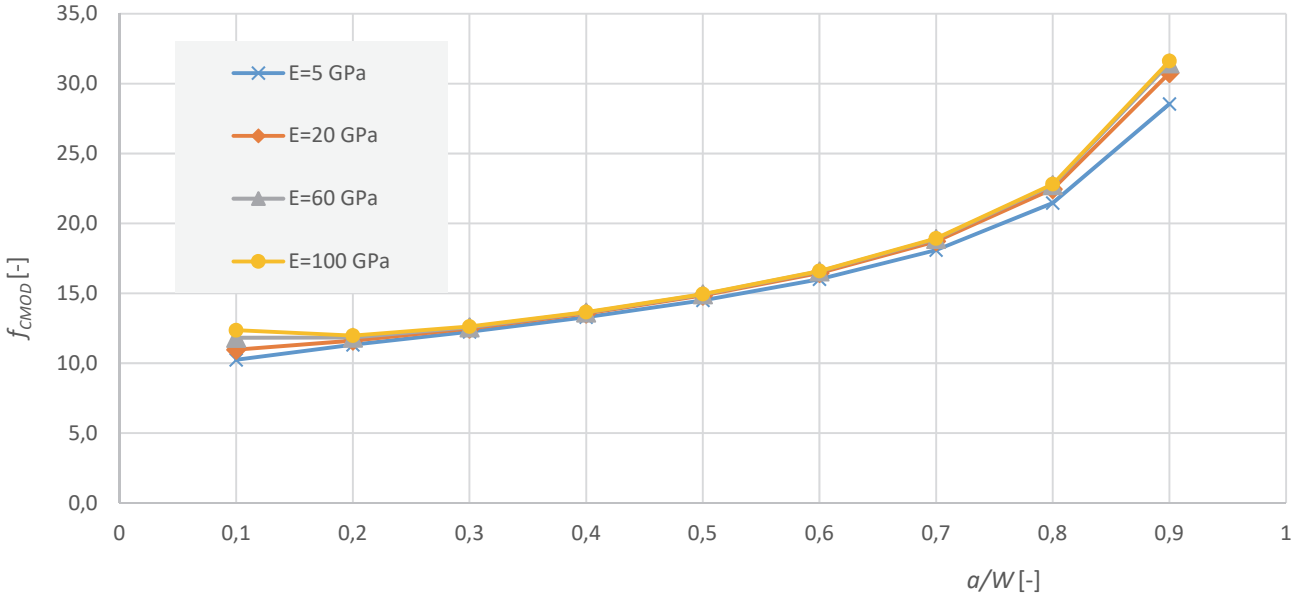

Figure 7: Values of CMOD (crack mouth open displacement) versus a/W, the effect of elasticity modulus ratio (steel E=210 GPa).

Compliance functions (according Eqs. (4) and (5)) for opening displacement under the loading force (COD) and for opening displacement at the crack mouth (CMOD) follow for Young's modulus of concrete E=5, 20 and 100 GPa, respectively:

for COD

$$f_{COD}\ (E=5) = 6.0419 - 4.4767\alpha + 77.12\alpha^2 - 153.38\alpha^3 + 106.59\alpha^4 \quad (11)$$

$$f_{COD}\ (E=20) = 6.7211 - 12.764\alpha + 111.24\alpha^2 - 208.43\alpha^3 + 138.35\alpha^4 \quad (12)$$

$$f_{COD}\ (E=100) = 7.491 + 21.077\alpha + 139.81\alpha^2 - 248.63\alpha^3 + 158.95\alpha^4 \quad (13)$$

and for CMOD

$$f_{CMOD}\ (E=5) = 10.54 - 10.549\alpha + 100.94\alpha^2 - 194.05\alpha^3 + 132.77\alpha^4 \quad (14)$$

$$f_{CMOD}\ (E=20) = 12.478 - 27.907\alpha + 162.68\alpha^2 - 285.45\alpha^3 + 182.31\alpha^4 \quad (15)$$

$$f_{CMOD}\ (E=100) = 15.905 - 55.717\alpha + 245.61\alpha^2 - 390.95\alpha^3 + 231.39\alpha^4 \quad (16)$$

Effect of 2D and 3D model solutions

The results of 2D and 3D model solutions (steel E=210 GPa, concrete E=25 GPa) are shown in Figs. 9-12 (stress intensity factor, T-stress, COD and CMOD). The model of 3D model solution was prepared as ¼ of all body, the steel part was as ½ of the round bar. The example of the model after deformation is shown in Fig. 8.

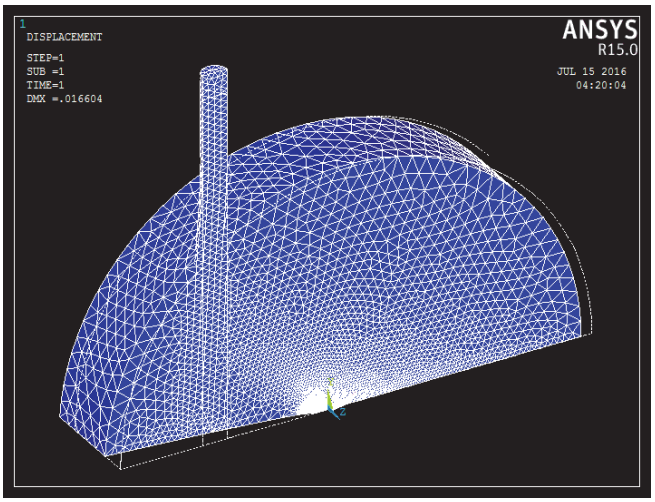

Figure 8: Example of 3D finite element model after deformation.

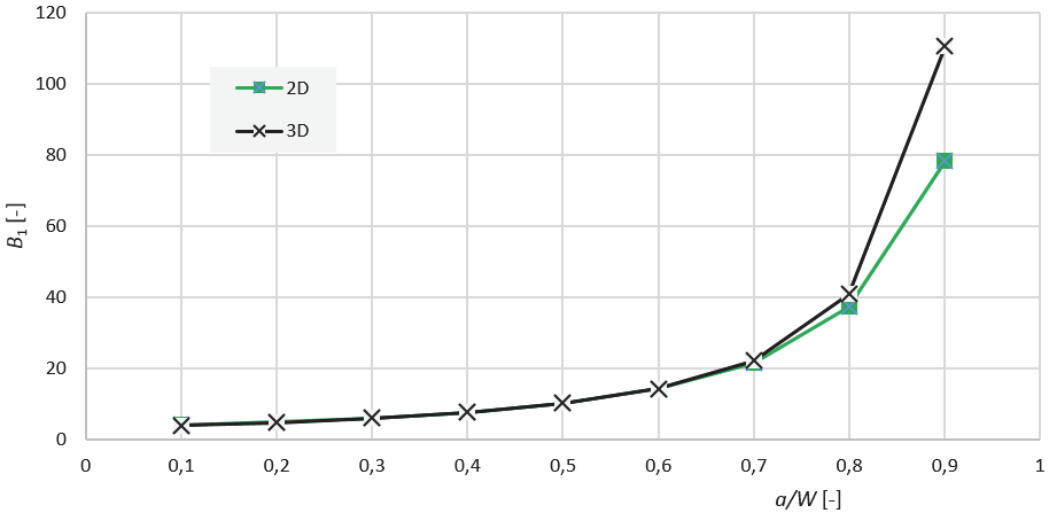

Figure 9: Values of dimensionless B_1 factor (stress intensity factor) versus a/W, effect of elasticity modulus ratio (steel E=210 GPa).

The B_1 curves are practically the same for both cases. It only changes for values of relative crack length longer than α =0.7 (see in Fig. 9). The functions of calibration curve for both (2D and 3D) solutions (with Young's modulus of concrete E= 25 GPa) can be introduced as follows:

$$B_1 \text{ (2D)} = -4.4888 + 157.35\alpha - 992.61\alpha^2 + 2913.2\alpha^3 - 3845.6\alpha^4 + 1937.8\alpha^5 \quad (17)$$

$$B_1 \text{ (3D)} = -19.17 + 437.74\alpha - 2795.2\alpha^2 + 7977.5\alpha^3 - 10259\alpha^4 + 4936.2\alpha^5 \quad (18)$$

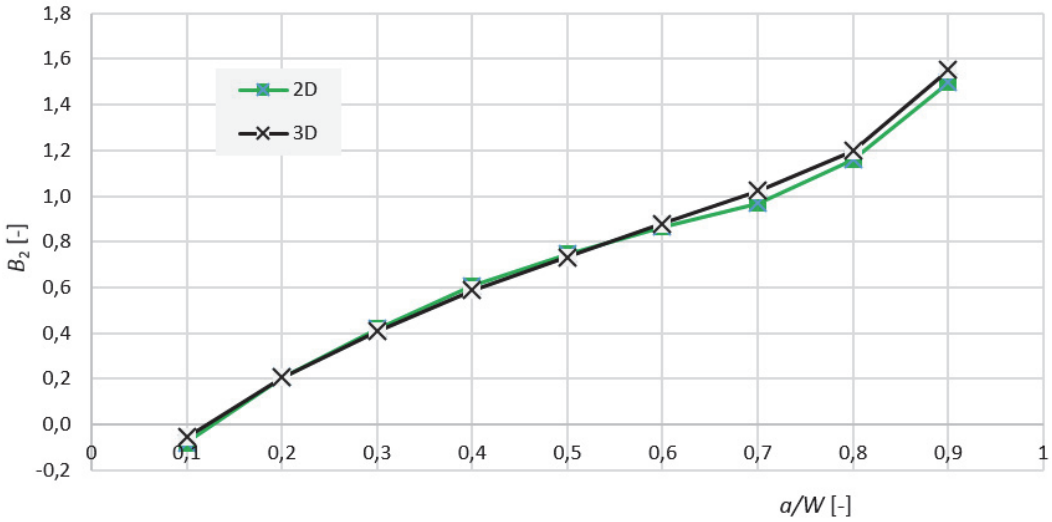

Figure 10: Values of dimensionless B_2 factor (T-stress) versus a/W, the effect of elasticity modulus ratio (steel E=210 GPa).

Fig. 10 shows that the B_2 parameter changes practically negligibly. Only for very long cracks 0.7 and longer, some differences can be seen between curves.

$$B_2 \text{ (2D)} = -0.352 + 2.6238\alpha + 2.2014\alpha^2 - 9.8235\alpha^3 + 7.4131\alpha^4 \quad (19)$$

$$B_2 \text{ (3D)} = -0.2905 + 2.2439\alpha + 2.305\alpha^2 - 8.4968\alpha^3 + 6.315\alpha^4 \quad (20)$$

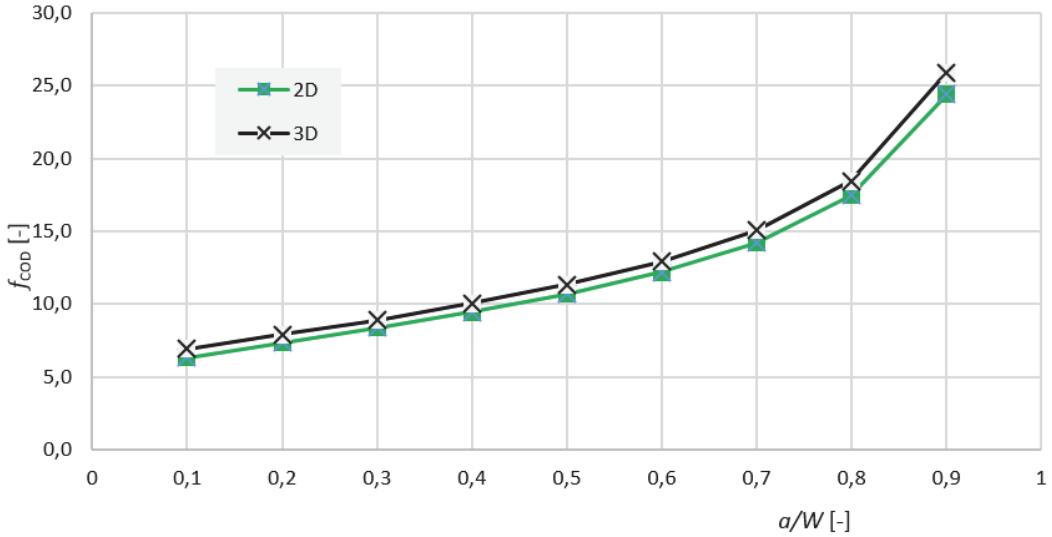

Figure 11: Values of COD (opening at load line) versus a/W, the effect of elasticity modulus ratio (steel E=210 GPa).

The curves obtained by 3D model solution do not differ very much and they follow the shape of ones obtained by 2D model solution. The main differences come for relative long crack α=0.8 for the values of stress intensity factor results, see

Fig. 9. The obtained values are a little higher over a whole range of relative crack length and that's caused by τ stress component.
Compliance functions for opening displacement under the loading force (COD) and for opening displacement at the crack mouth (CMOD) (according Eqs. (4) and (5)) follow from 2D and 3D model solutions, respectively:

for COD

$$f_{COD}\,(2D) = 6.8209 - 13.922\alpha + 115.54\alpha^2 - 214.86\alpha^3 + 141.81\alpha^4 \quad (21)$$

$$f_{COD}\,(3D) = 7.7038 - 18.056\alpha + 131.72\alpha^2 - 239.55\alpha^3 + 155.85\alpha^4 \quad (22)$$

and for CMOD

$$f_{CMOD}\,(2D) = 12.849 - 31.071\alpha + 172.7\alpha^2 - 298.93\alpha^3 + 188.98\alpha^4 \quad (23)$$

$$f_{CMOD}\,(3D) = 15.138 - 43.207\alpha + 210.8\alpha^2 - 350.23\alpha^3 + 215.04\alpha^4 \quad (24)$$

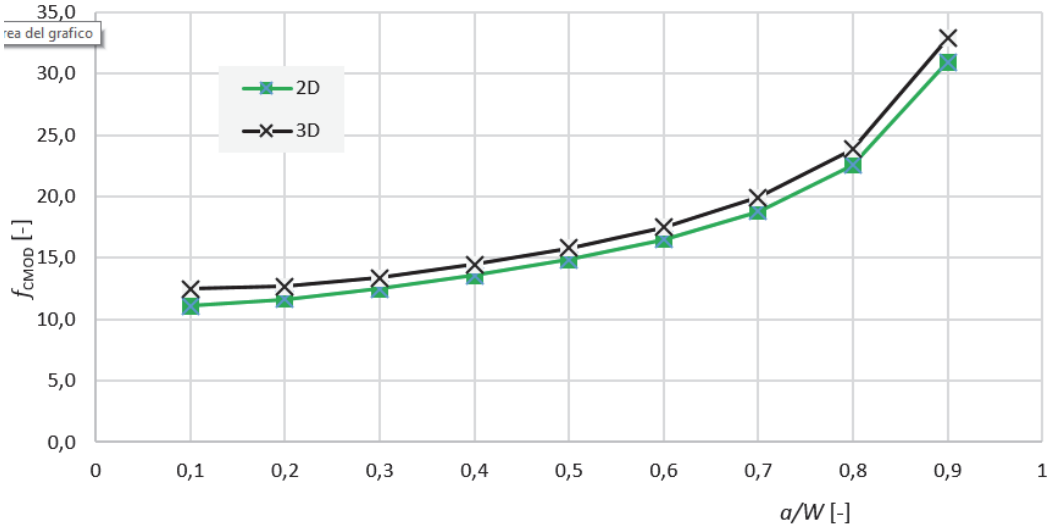

Figure 12: Values of CMOD (crack mouth open displacement) versus a/W, the effect of elasticity modulus ratio (steel E=210 GPa).

CONCLUSIONS

The finite element analysis of two effects on modified compact tension test for specimens like concrete is introduced by means of a constraint-based two parameter fracture mechanic approach. Five various materials configurations (steel and concrete) and 2D and 3D solutions were investigated. The following principal conclusions could be derived:

- The influence of elasticity modulus ratio (constant value of Young's modulus defined for steel and different values for concrete) on the calibration curve is not negligible and for each case a different polynomial function has to be used.
- The curves obtained by 3D model solution don't differ very much and they follow the shape of ones obtained with 2D model solution very well, the largest differences are related to long crack in stress intensity factor results. The obtained values are a little higher over a whole range of relative crack length and that's caused by τ stress component.
- The results from 2D model solution can be used instead of ones from 3D model solution and they are in a range of acceptance. Moreover, they can be calculated much faster for another specimen sizes or bars positions.

ACKNOWLEDGEMENT

This paper has been worked out under the "National Sustainability Programme I" project "AdMaS UP – Advanced Materials, Structures and Technologies" (No. LO1408) supported by the Ministry of Education, Youth and Sports of the Czech Republic.

REFERENCES

[1] Anderson, T., L. Fracture mechanics fundamentals and applications, CRC Press (1991)
[2] ANSYS Reference, www.ansys.com
[3] ASTM E399 - 12e3 Standard Test Method for Linear-Elastic Plane-Strain Fracture Toughness KIc of Metallic Materials, DOI: 10.1520/E0399.
[4] Cifuentes, H., Lozano, M., Holušová, T., Medina, F., Seitl, S., and Canteli, A. Applicability of a modified compact tension specimen for measuring the fracture energy of concrete, Anales de Mecánica de la Fractura, 32 (2015) 208–213.
[5] Fernández-Canteli, A., Castañón, L., Nieto, B., Lozano, M., Holušová, T., Seitl, S. Determining fracture energy parameters of concrete from the modified compact tension test, Frattura ed Integrità Strutturale, 30 (2014) 383–393. DOI: 10.3221/IGF-ESIS.30.46.
[6] Gaedicke, C., Marines, A., Miankodila, F., Assessing the abrasion resistance of cores in virgin and recycled aggregate pervious concrete, Construction and Building Materials, 68 (2014) 701-708. DOI: 10.1016/j.conbuildmat.2014.07.001
[7] Gaedicke, C., Torres, A., Huynh K.C.T., Marines, A., A method to correlate splitting tensile strength and compressive strength and compressive strength of pevious concrete and cores, Construction and Building Materials 125(2016) 271–278. DOI: 0.1016/j.conbuildmat.2016.08.031.
[8] Hidayat, A., Purwanto, P., Puspowardojo, J., Aziz, F.A., The influence of graded concrete strength on concrete element, Procedia Engineering, 125(2015) 1023–1029. DOI**:** 10.1016/j.proeng.2015.11.157
[9] Holušová, T., Lozano, M., Canteli, A., Komárková, T., Kocáb, D., Seitl, S. Influence of the gripping fixture on modified compact tension test results: evaluation of the experiments on cylindrical concrete specimens, Transactions of the VŠB – Ostrava Technical University of Ostrava Civil Engineering Series, 15(2) (2015) 10. DOI: 10.1515/tvsb-2015-0010.
[10] Holušová, T., Seitl, S., Canteli, A. Numerical Simulation of Modified Compact Tension Test depicting of Experimental Measurement by ARAMIS, Key Engineering Materials 627 (2015) 277–280. DOI: 10.4028/www.scientific.net/KEM.627.277
[11] Knésl, Z., Bednář, K. Two Parameter fracture mechanics: Calculation of parameters and their values, Institute of Physics of Materials Academy of Science of the Czech Republic, (1998).
[12] Korte, S., Boel, V., De Corte, W., De Schutter, G., Static and fatigue mechanics properties of self-compacting concrete using three-point bending tests and wedge-splitting tests, Construction and Building Materials, 57(2014) 1–8. DOI: 10.1016/j.conbuildmat.2014.01.090.
[13] Leevers, P.S., Radon, J.C., Inherent stress biaxiality in various fracture specimen geometries, International Jouirnal of Fracture, 19(4) (1982) 311–325. DOI: 10.1007/BF00012486.
[14] Merta, I., Tschegg, E.K., Fracture energy of natural fibre reinforced concrete, Construction and Building Materials, 40 (2013) 991–997. doi:10.1016/j.conbuildmat.2012.11.060.
[15] Mynarcik, P., Core Sampling for fiber concrete constructions-Context between quantity of core samples and evaluation of fiber concrete characteristics, Procedia Engineering 114 (2015) 493–499. DOI:10.1016/j.proeng.2015.08.097.
[16] Ponikiewski, T., Katzer, J., Properties of fresh SCC mix reinforced by different types of steel and polymer fibre, Construction and Building Materials, 62 (2014) 96–101. DOI: 10.1016/j.conbuildmat.2014.03.037.
[17] RILEM Publications SARL, Determination of the fracture energy of mortar and concrete by means of three-point bend tests on notched beams, (1985) 285–290.
[18] RILEM TC 162-TDF: Test and Design Methods for Steel Fibre Reinforced Concrete, Bending test, Materials and Structure, 35 (2002) 579–582.
[19] Řoutil, L., Veselý, V., Seitl, S. Fracture analysis of cube- and cylinder- shaped WST specimens made of cementitious composites with various characteristic length, 188-489 (2012) 533–536. DOI: 10.4028/www.scientific.net/KEM.488-489.533.

[20] Seitl, S., Veselý, V., Řoutil, L., Two-parameter fracture mechanical analysis of a near-crack-tip stress field in wedge splitting test specimens, Computers and Structures, 21-22 (2011) 1852–1858. DOI: 10.1016/j.compstruc.2011.05.020.
[21] Seitl, S., Viszlay, V., Cifuentes, H., Canteli, A. Effects of specimen size and crack depth ratio on calibration curves for modified compact tension specimens, Transactions of the VŠB – Technical University of Ostrava Civil Engineering Series, 15(2), (2015) 23. DOI: 10.1515/tvsb-2015-0023.
[22] Tada, H., Paris P.C., Irwin, R.G. The Stress Analysis of Cracks Handbook (3rd Edition). New York: ASM International, (2000).
[23] Veselý, V., Sobek, J., Numerical study of failure of cementitious composite specimens in modified compact tension fracture test, Transactions of the VŠB – Technical University of Ostrava, Civil Engineering Series, 13(2) (2013) 180–187, DOI: 10.2478/tvsb-2013-0025,
[24] Wu, Y., Xu, S., Li, Q., Ruiz, G., Yu, R.C., Estimation of real fracture parameters of a dam concrete with large size aggregates through wedge splitting tests of drilled cylindrical specimens, Engineering Fracture Mechanics, (2016). DOI: 10.1016/j.engfracmech.2016.06.012.